Measured Millimeter-Wave Channels in Corridor Scenarios with Large-Scale Antenna Arrays

Mbugua, Allan Wainaina; Fan, Wei; Zhang, Fengchun; Chen, Yun; Pedersen, Gert Frølund

Published in:
2020 14th European Conference on Antennas and Propagation (EuCAP)

DOI (link to publication from Publisher):
10.23919/EuCAP48036.2020.9135660

Publication date:
2020

Document Version
Accepted author manuscript, peer reviewed version

Measured Millimeter-Wave Channels in Corridor Scenarios with Large-Scale Antenna Arrays

Allan Wainaina Mbugua*†, Wei Fan*, Fengchun Zhang* Yun Chen†, Gert Frølund Pedersen*
*Department of Electronic Systems, Antennas, Propagation and Millimeter-wave Systems (APMS) Section,
Aalborg University, Aalborg, 9220, Denmark.
†Huawei Technologies Duesseldorf GmbH, Munich Research Center, Munich, 80992, Germany.

Email: *{awm,wfa,fz,gfp}@es.aau.dk

***Abstract*—In this paper, measured millimeter-wave (mm-wave) channels with two large-scale antenna arrays in a corridor scenario are presented. The measurements were carried out using a radio-over-fiber (RoF) based vector network analyzer (VNA) channel sounder with a virtual uniform circular array (UCA) and a uniform rectangular array (URA) in a line-of-sight (LoS) scenario. The spatial-temporal characteristics of the channel are then obtained using the Bartlett beamformer and frequency invariant beamforming (FIBF) algorithms for the URA and UCA, respectively. The high dynamic range of the channel sounder coupled with the high spatial resolution of the large scale arrays enable the extraction of weak multipath components (MPC)s as well as MPCs arriving with a long delay.**

***Index Terms*—antennas, millimeter-wave, propagation, radio-over-fiber,virtual arrays.**

I. Introduction

The spectral crowding at sub-6 GHz has spurred research in the millimeter-wave (mm-wave) frequency bands which are the candidate bands for the fifth generation (5G) mobile network. The availability of large unallocated bandwidth at mm-wave bands is seen as a key enabler to achieving high data rates expected in 5G networks. Moreover, the small wavelength at mm-wave bands enable the implementation of electrically large antenna arrays in compact form. This leads to an increase in the spatial resolution which is crucial in separation of users in crowded scenarios [1].

Channel measurements in realistic propagation scenarios are thus fundamental for accurate characterization of mm-wave channels [2]. Moreover, channel measurements are pivotal for calibration and validation of mm-wave channel models. However, mm-wave channels are characterized by high free space propagation loss and high signal loss in the electronic hardware which limits the practical measurement range. The use of high gain antennas and large-scale antenna arrays is thus fundamental to combat the high path loss in channel sounding campaigns [3]. On the other hand, signal loss due to hardware impairments in channel sounders at mm-wave frequencies can be mitigated by the use of radio-over-fiber (RoF) techniques or frequency up-converters and down-converters [4], [5], [6].

To obtain the channel spatio-temporal characteristics, the antenna array configurations commonly employed in the literature are the uniform circular array (UCA) and the uniform rectangular array (URA). The attractive features of the employing UCA is that it has a uniform beam pattern in the azimuth which is crucial when omni-directional spatio-temporal channel information is needed. In addition the UCA has a uniform sidelobe level in a 360° steering range [7]. However, the UCA suffers from joint sidelobes in angle and delay domain when using the Bartlett beamformer. On the other hand, the URA is attractive as it enables the use of robust beamforming algorithms e.g. the Barlett beamformer.

In this paper the spatio-temporal characteristics of a long corridor environment are presented. Channel measurements are performed using a virtual UCA and URA coupled to a vector network analyzer (VNA) in a line-of-sight (LoS) scenario. Channel estimation for the URA is obtained using the Bartlett beamformer whereas the channel estimation for the UCA is obtained using the frequency invariant beamforming (FIBF) algorithm. The FIBF algorithm has an invariant beam pattern with frequency and eliminates the joint sidelobes in angle and delay domain which are observed when using the Bartlett beamformer [8], [9].

II. Measurement Setup

A. Measurement System

The measurement system utilized is a RoF based VNA channel sounder [6]. The use of RoF techniques mitigate the signal loss in conventional coaxial cable based VNA channel sounders which can be as high 1.59 dB/m at 30 GHz. The reduction in the radio frequency (RF) signal loss when using RoF techniques can be up to 0.8 dB/km for single mode optical cable. This reduction in the signal loss enables a back-to-back dynamic range of 112 dB at 30 GHz. The block diagram of the channel sounder is shown in Fig. 1. The transmitter (Tx) [10] and receiver (Rx) (A-INFO-SZ-2003000/P) antennas are vertically polarized with an omni-directional pattern in the azimuth.

B. Measurement Settings

The virtual UCA and URA have an inter-element spacing of 0.44λ and 0.4λ respectively, where λ is the wavelength at 30 GHz. The measurements are performed in the frequency band from 26.5 GHz to 30 GHz with an intermediate frequency (IF) bandwidth of 5 kHz. For the measurement campaign with the UCA, the Tx and Rx antennas are placed at a height of

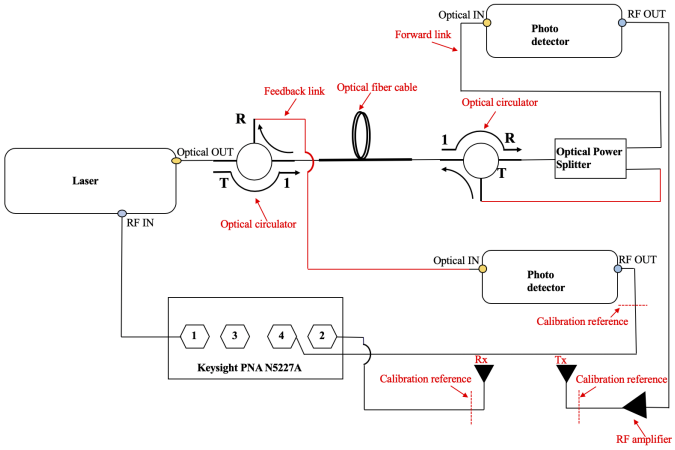

Fig. 1. Block diagram of the RoF based VNA channel sounder.

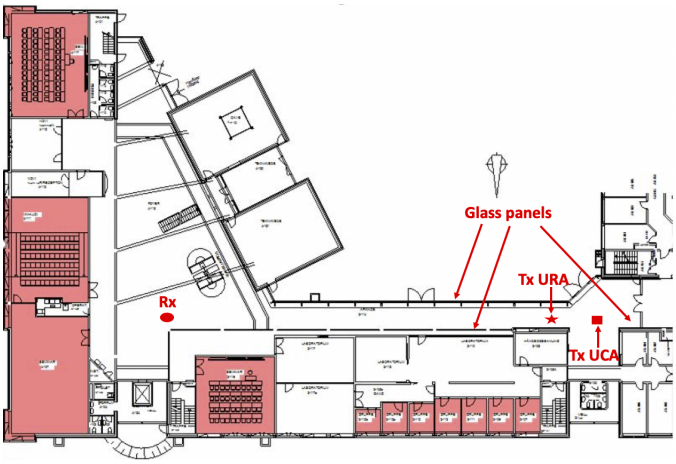

Fig. 2. Placement of the Tx and Rx antenna in relation to the floor plan.

1.23 m whereas for the measurement URA measurement the height is 1.61 m. The center of the antennas were laser aligned to ensure the elevation direction of the main beam is on the same azimuth plane since the antennas have a narrow beam in the elevation. The VNA settings and measurement parameters are summarized in Table I.

TABLE I
MEASUREMENT PARAMETERS

Parameter	UCA	URA
VNA Tx power	-12 dBm	-12 dBm
VNA sweep time	2.003 s	2.003 s
Frequency band	26.5 GHz to 30 GHz	26.5 GHz to 30 GHz
Delay resolution	0.29 ns	0.29 ns
IF bandwidth	5 kHz	5 kHz
Frequency points	6000	6000
Array elements	720	900
Inter-element spacing	0.44λ	0.4λ
Array dimensions	(radius) 50 cm	11.6 cm $\times$ 11.6 cm
Tx, Rx height	1.23 m	1.61 m

C. Measurement Scenario

The measurements are carried out in a LoS corridor scenario shown in Fig. 3 with the Rx and Tx antennas placed at the opposite ends of the corridor. The corridor is partly made of glass panels, steel pillars and brick walls on both sides. Behind the Rx antenna there is a concrete wall and behind the Tx antenna there is a door made of glass. The floor plan of the corridor scenario is illustrated in Fig. 2. The Tx and Rx antennas are separated by a distance of 53 m and 46 m for the virtual UCA and URA measurements respectively. The placement of the antennas is illustrated in Fig. 3 for the UCA scenario.

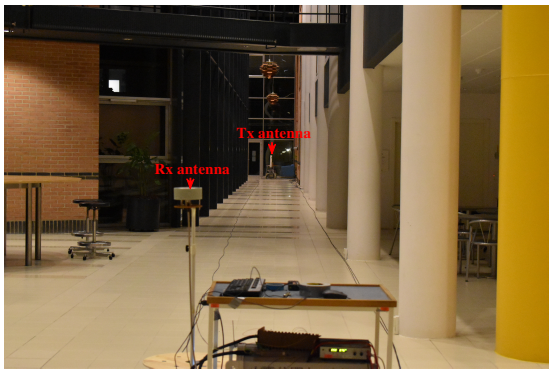

(a)

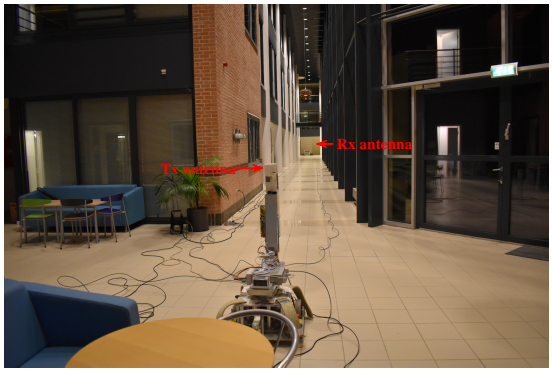

(b)

Fig. 3. Photo of the measurement scenario. (a) View from the Rx antenna and (b) view from the Tx antenna.

III. Signal Model

Considering an arbitrary antenna array with *P* omni-directional antenna elements and that the far-field assumption holds, then the phase difference between consecutive antenna array elements is due to the propagation delay of the impinging wave on the antenna array. The channel frequency response (CFR) at the origin of the arbitrary array can be obtained as a sum of the *K* plane waves impinging on the array

$$H(f) = \sum_{k=1}^{K} \alpha_k e^{-j2\pi f \tau_k} \tag{1}$$

where *f* is the frequency, α_k and τ_k are the amplitude and the delay of the *k-th* plane wave.

The frequency response at the *p-th* antenna element in the array is simply a phase shifted version of $H(f)$ due to the propagation delay τ_p from the origin to the *p-th* antenna element of the *k-th* plane wave with azimuth angle of arrival (AoA) φ_k and elevation AoA θ_k.

$$H_p(f) = \sum_{k=1}^{K} \alpha_k e^{-j2\pi f(\tau_k + \tau_p)} \tag{2}$$

A. UCA

For a UCA of radius *r* with the origin at the center of the array, the propagation delay τ_p in (2) can be obtained as:

$$\tau_p = -\frac{r \cdot \sin(\theta_k) \cdot \cos(\phi_p - \varphi_k)}{c} \tag{3}$$

where *c* is the speed of light in free space and ϕ_p the location of the *p-th* antenna element which can be calculated as:

$$\phi_p = \frac{2\pi \cdot (p-1)}{P} \tag{4}$$

The antenna array frequency response $H_A(f, \theta, \varphi)$ can be obtained as:

$$H_A(f, \theta, \varphi) = \sum_{k=1}^{K} v_k(f, \theta, \varphi) \cdot H(f) \tag{5}$$

where $v_k(f, \theta, \varphi)$ is the unit frequency invariant array beam pattern using the compensation filter $\hat{G}_m(f)$ of the FIBF algorithm in [8].

B. URA Signal Model

The virtual URA considered is composed of P_x and P_y elements in the *x-axis* and the *y-axis*, respectively. The propagation delay τ_p in (2) for the URA can then be obtained as:

$$\tau_p = -\frac{\mathbf{u}_p \cdot \hat{\mathbf{v}}(\theta_k, \varphi_k)}{c} \tag{6}$$

where $\mathbf{u}_p$ is the position vector of the *p-th* antenna element which is defined as:

$$\mathbf{u}_p = \begin{bmatrix} d(P_x - 1) \\ d(P_y - 1) \\ 0 \end{bmatrix} \tag{7}$$

where *d* is the antenna inter-element spacing and $\hat{\mathbf{v}}(\theta_k, \varphi_k)$ is the unit vector in the direction (θ_k, φ_k) which is defined as

$$\hat{\mathbf{v}}(\theta_k, \varphi_k) = \begin{bmatrix} \sin(\theta_k)\cos(\varphi_k) \\ \sin(\theta_k)\sin(\varphi_k) \\ \cos(\theta_k) \end{bmatrix} \tag{8}$$

The antenna array frequency response $H_A(f, \theta, \varphi)$ is then obtained by aligning each antenna element frequency response $H_p(f)$ to the origin using the respective complex weight w_p.

$$H_A(f, \theta, \varphi) = \frac{1}{P_x}\frac{1}{P_y} \sum_{x=0}^{P_x-1} \sum_{y=0}^{P_y-1} w_p(f, \theta, \varphi) H_p(f) \tag{9}$$

where $w_p(f, \theta, \varphi)$ is defined as

$$w_p(f, \theta, \varphi) = e^{\frac{-j2\pi}{\lambda} \mathbf{u}_{x,y} \cdot \hat{\mathbf{v}}(\theta_k, \varphi_k)} \tag{10}$$

with λ the wavelength. The channel impulse response (CIR) $h(\tau, \theta, \varphi)$ can then be obtained by taking the inverse discrete Fourier transform of the antenna array frequency response $H(f, \theta, \varphi)$

$$h(\tau, \theta, \varphi) = \sum_{n=0}^{N-1} H(f_n, \theta, \varphi) e^{j2\pi f_n \tau} \tag{11}$$

f_n is the *n-th* frequency bin.

IV. Measurement Results

The power delay profile (PDP) of the channel at each antenna element position of the UCA is shown in Fig. 4a. The channel is characterized by few dominant multipath components (MPC)s and several MPCs that decay after a delay of 300 ns. In addition, two dominant MPCs (path 4 and 5) delayed in time can be observed after a delay of 600 ns. The power angle delay profile (PADP) obtained with the FIBF algorithm, is shown in Fig. 4b. The joint sidelobes in delay and angle domain are suppressed in comparison to the PADP obtained for a UCA in [11]. The channel is also observed to be highly directional with the LoS having an AoA of 360° and the most significant MPCs, path 2 having an AoA of 180°. The AoA of the other dominant MPCs path 3, 4 and 5 is 180°, 360° and 180° respectively. This indicates that these dominant MPCs (path 2, 3, 4 and 5) are specular reflections of the LoS component. Path 2 is most likely a first order reflection from the glass door behind the Tx antenna while path 4 is a first order reflection from the wall behind the Rx antenna. On the other hand, path 5 can be a seen to be a second order specular reflection emanating from the wall behind the Rx antenna.

The PDP of the measured channel with the URA is shown in Fig. 5a. The channel exhibits similar characteristics as those observed with the UCA measurements. The power of the MPCs decays around 300 ns and the tail of the PDP is characterized by MPCs delayed in time. The spatio-temporal characteristics also closely resemble the PADP obtained with the UCA as illustrated in Fig. 5b. The dominant MPCs lie in two main AoA directions 270° (LoS and path 3) and 90° (path 2 and 4). The difference in AoA of the MPC in the two

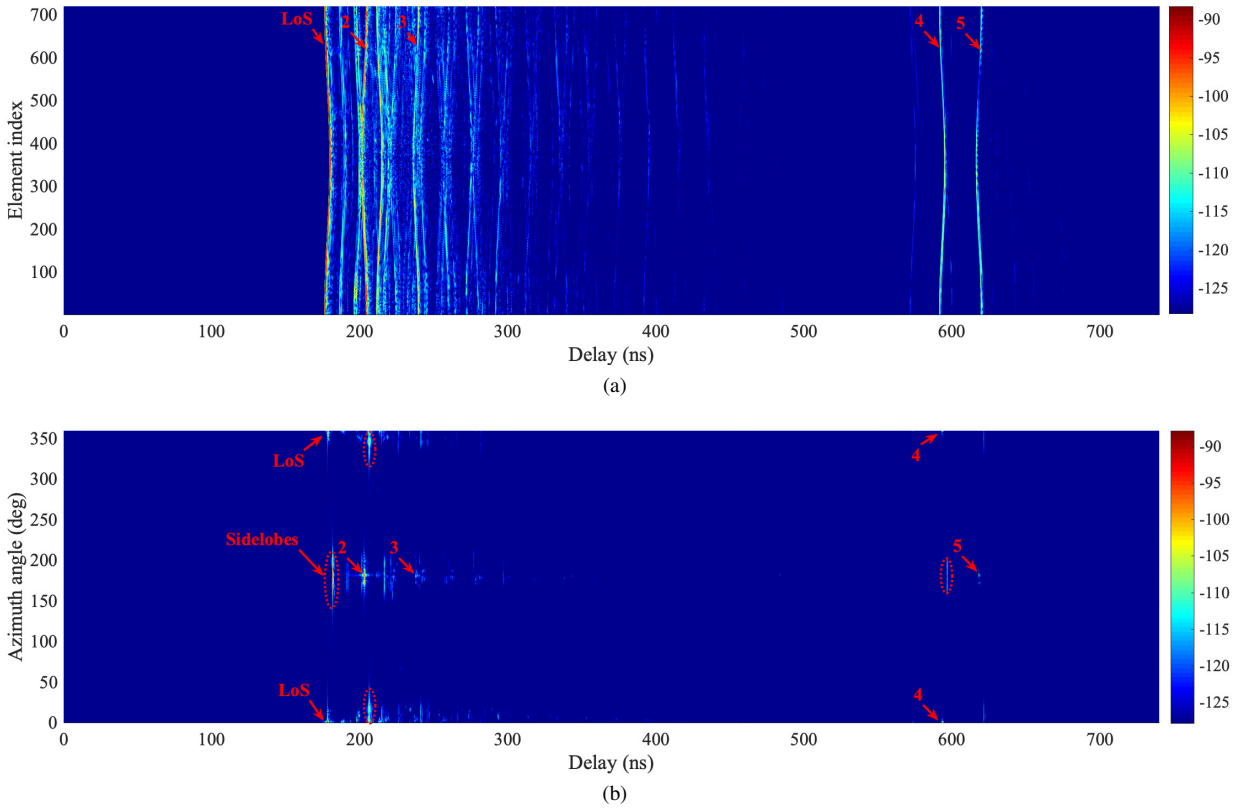

Fig. 4. Channel measurement on a 53 m corridor with the UCA. The power dynamic range is limited to 40 dB. (a) Measured PDP and (b) the PADP where the sidelobes are outined in the dotted ellipse.

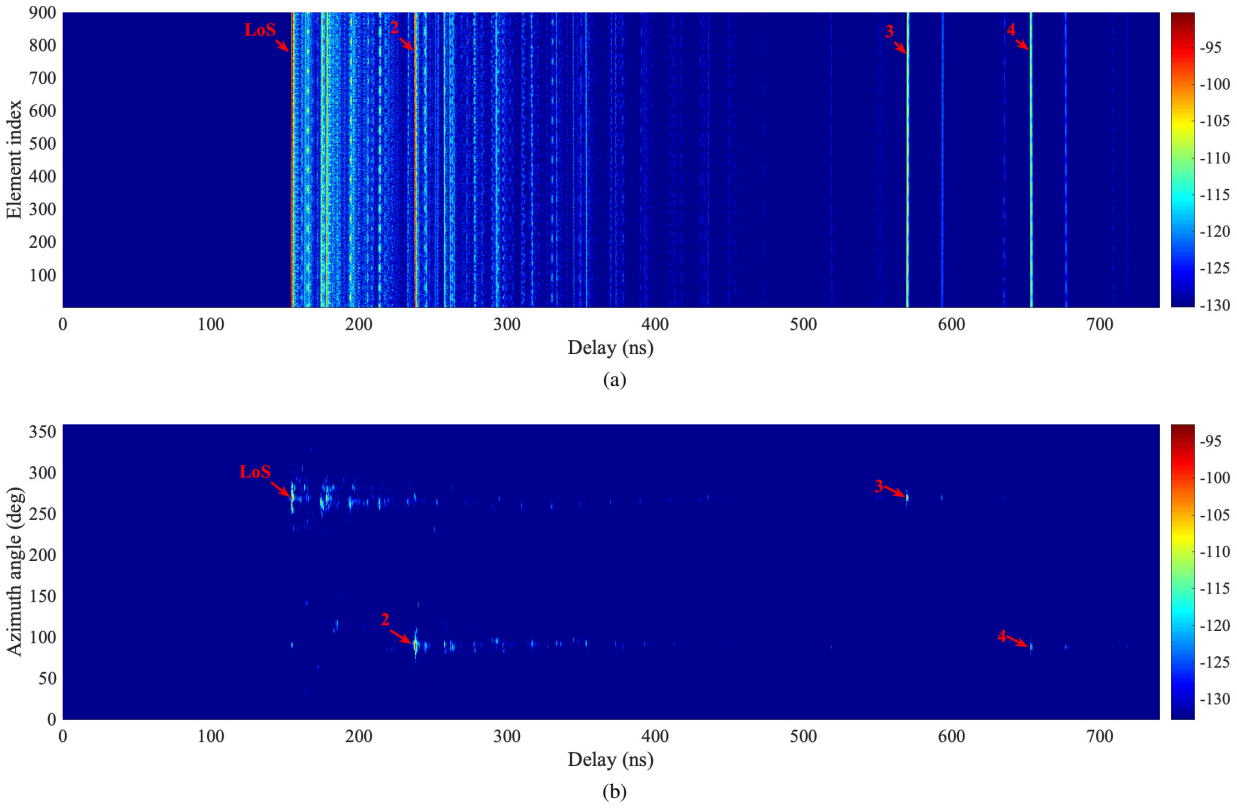

Fig. 5. Channel measurement on a 46 m corridor with a URA.The power dynamic range is limited to 40 dB. (a) Measured PDP and (b) the PADP.

antenna arrays is due different choice of the origin for the antenna configuration.

In the corridor measurement with URA, the channel parameters are seen to be stationary across the array for the dominant MPCs as well as the weak MPCs as shown in Fig. 5a. For the UCA measurement stationarity of the channel parameters can also be observed for the dominant MPCs as illustrated in Fig. 4a. However, for the weak MPCs with a selected dynamic range of 40 dB, non-stationarity of channel parameters across the antenna array can be observed. The displayed difference in the stationarity of channel parameters across the two antenna arrays could be due to the significant difference in the electrical size of the arrays.

V. Conclusion

This paper presented the channel measurement results in a long corridor environment using two types of large scale antenna arrays. The high dynamic range of the RoF based VNA channel sounder enabled the extraction of delayed MPCs as well as weak MPCs. For the LoS scenario and a dynamic range of 40 dB, the channel parameters display stationarity across the array for the dominant components with non-stationarity being observed in the electrically larger UCA for the weak MPCs.

Acknowledgment

This work was supported by Huawei Technologies.

References

[1] J. Flordelis, F. Rusek, X. Gao, G. Dahman, O. Edfors, and F. Tufvesson, "Spatial separation of closely-located users in measured massive mimo channels," *IEEE Access*, vol. 6, pp. 40 253–40 266, 2018.

[2] R. He, B. Ai, G. L. Stber, G. Wang, and Z. Zhong, "Geometrical-based modeling for millimeter-wave mimo mobile-to-mobile channels," *IEEE Trans. Veh. Technol.*, vol. 67, no. 4, pp. 2848–2863, April 2018.

[3] W. Roh, J. Seol, J. Park, B. Lee, J. Lee, Y. Kim, J. Cho, K. Cheun, and F. Aryanfar, "Millimeter-Wave Beamforming as an Enabling Technology for 5G Cellular Communications: Theoretical Feasibility and Prototype Results," *IEEE Commun. Mag.*, vol. 52, no. 2, pp. 106–113, February 2014.

[4] J. Hejselbaek, Y. Ji, W. Fan, and G. F. Pedersen, "Channel Sounding System for MM-Wave Bands and Characterization of Indoor Propagation at 28 GHz," *Int. J. Wireless Inf. Netw.*, vol. 24, no. 3, pp. 204–216, Sep 2017.

[5] B. N. Liya and D. G. Michelson, "Characterization of Multipath Persistence in Device-to-Device Scenarios at 30 GHz," in *Proc. IEEE Globecom Workshops (GC Wkshps)*, Dec 2016, pp. 1–6.

[6] A. Mbugua, W. Fan, K. Olesen, X. Cai, and G. Pedersen, "Phase Compensated Optical Fiber Based Ultra-Wideband Channel Sounder," *IEEE Trans. Microw. Theory Techn.*, in press 2019.

[7] P. Ioannides and C. A. Balanis, "Uniform Circular and Rectangular Arrays for Adaptive Beamforming Applications," *IEEE Antennas Wireless Propag. Lett.*, vol. 4, pp. 351–354, 2005.

[8] F. Zhang, W. Fan, and G. F. Pedersen, "Frequency-Invariant Uniform Circular Array for Wideband mm-Wave Channel Characterization," *IEEE Antennas Wireless Propag. Lett.*, vol. 16, pp. 641–644, 2017.

[9] W. Fan, Y. Ji, F. Zhang, and G. F. Pedersen, "Channel Estimation Algorithms and Their Impact on Wideband Millimeter Wave Channel Characteristics," in *2nd URSI Atlantic Radio Science Meeting (AT-RASC)*, May 2018, pp. 1–4.

[10] S. S. Zhekov, A. Tatomirescu, and G. F. Pedersen, "Antenna for Ultrawideband Channel Sounding," *IEEE Antennas Wireless Propag. Lett.*, vol. 16, pp. 692–695, 2017.

[11] W. Fan, I. Llorente, J. Nielsen, K. Olesen, and G. Pedersen, "Measured Wideband Characteristics of Indoor Channels at Centimetric and Millimetric Bands," *EURASIP J. Wireless Commun. Netw.*, vol. 2016, no. 58, 2016, special issue on Radio Channel models for higher frequency bands.